Science of the Total Environment 579 (2017) 736–744

Contents lists available at ScienceDirect

Science of the Total Environment

journal homepage: www.elsevier.com/locate/scitotenv

Heteroaggregation of graphene oxide nanoparticles and kaolinite colloids

Nikolaos P. Sotirelis, Constantinos V. Chrysikopoulos *

School of Environmental Engineering, Technical University of Crete, 73100 Chania, Greece

HIGHLIGHTS

- Heteroaggregation between GO and KGa-1b is not favorable under normal conditions.
- High ionic strength and low pH values enhance the attachment of GO onto KGa-1b.
- The attachment of GO onto KGa-1b is exothermic and not spontaneous.
- GO−(KGa-1b) formation is attributed to surface charge changes of KGa-1b colloids.
- The CCC for the heteroaggregation between GO and KGa-1b is 152 mM NaCl.

GRAPHICAL ABSTRACT

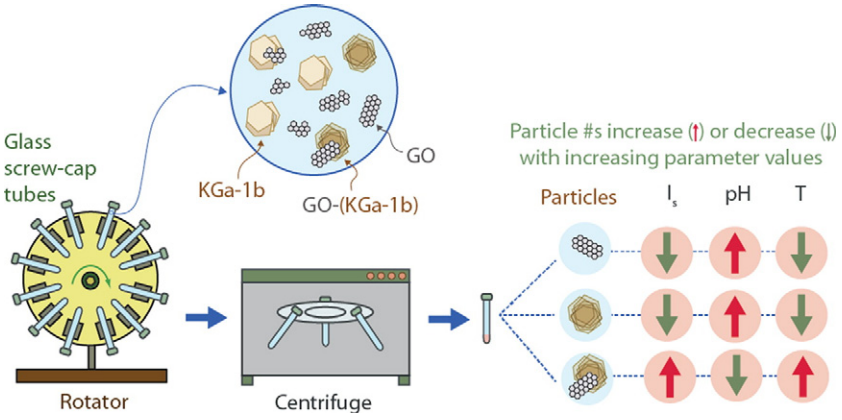

ARTICLE INFO

Article history:
Received 25 September 2016
Received in revised form 5 November 2016
Accepted 6 November 2016
Available online 22 November 2016

Editor: D. Barcelo

Keywords:
Graphene oxide
Nanoparticles
Attachment
Heteroaggregation
Kaolinite
Clays
Thermodynamics

ABSTRACT

Graphene oxide (GO) is a material with rapid production growth, and consequently GO nanoparticles are expected to eventually penetrate subsurface formations, where fine mineral particles are in abundance. This study examines the heteroaggregation of GO nanoparticles with kaolinite (KGa-1b) colloids under various conditions. Dynamic batch experiments were conducted in solutions with different pH values (pH = 4, 7, and 10), different ionic strengths (I_S = 7, 12, and 27 mM), and at three controlled temperatures (8, 14, and 25 °C). The experimental results showed that a relatively small amount of GO nanoparticles (5–20% of the initial concentration) attached immediately onto KGa-1b colloids, and reached equilibrium in <20 min. It was shown that neither temperature nor pH played a significant role in the attachment of GO nanoparticles onto KGa-1b colloids. In contrast, the attachment of GO nanoparticles onto KGa-1b colloids was shown to increase with increasing I_S. Additionally, time-resolved dynamic light scattering (DLS) was used to identify the influence of I_S on heteroaggregation between GO nanoparticles and KGa-1b colloids. The critical coagulation concentration (CCC) for the interaction between GO nanoparticles and KGa-1b colloids was 152 mM (NaCl). The interaction energies were calculated, for all experimental conditions, by using measured zeta potentials and applying the classical DLVO theory. The equilibrium experimental data were fitted with a Freundlich isotherm, and the attachment kinetics were described very well with a pseudo-second-order model. Furthermore, thermodynamic analysis revealed that the attachment process was nonspontaneous and exothermic.

1. Introduction

The growing production of engineered nanomaterials and their use in a wide range of engineering applications and commercial products

* Corresponding author.
E-mail address: cvc@enveng.tuc.gr (C.V. Chrysikopoulos).

http://dx.doi.org/10.1016/j.scitotenv.2016.11.034
0048-9697/

increased the probability of their emissions into environmental systems (Mueller and Nowack, 2008; Gottschalk et al., 2009, 2010; Keller et al., 2013; Keller and Lazareva, 2014). Because of the direct or indirect release of nanoparticles in the environment, numerous nanoparticles are detected in soil, water and air (Brar et al., 2010). Consequently, understanding thoroughly the fate and transport of nanoparticles in environmental systems and the related human health implications, is of paramount importance (Klaine et al., 2012; Sasidharana et al., 2014).

One very promising nanomaterial is graphene oxide (GO), which is a two-dimensional graphene-layered nanomaterial, composed of oxygen-bearing functional groups (Dreyer et al., 2010; Kim et al., 2012). Because of its excellent physiochemical properties, GO is used in a wide range of applications in various fields, including electrochemistry (Chen et al., 2012), biomedicine (Chung et al., 2013), energy storage (Lightcap and Kamat, 2013), and catalysis (Pyun, 2011). Numerous laboratory investigations have suggested that GO nanoparticles are toxic to a variety of mammalian organisms, as well as to bacterial cells (Akhavan and Ghaderi, 2010; Wang et al., 2011; Chang et al., 2011; Vallabani et al., 2011; Singh et al., 2011; Seabra et al., 2014; Hu et al., 2015). To assess these potential risks, the GO fate and transport in environmental systems and particularly in subsurface formations, where the migration behavior of nanoparticles is relatively complex, should be carefully investigated (Klaine et al., 2012; Lanphere et al., 2014; Zhou et al., 2016). Furthermore, the stability of GO nanoparticles plays significant role on their fate and transport in underground water environment. Many studies have explored the effect of solution chemistry (e.g. pH, ionic strength, cation valence, nanoparticle concentration, presence of organic matter) on GO nanoparticles aggregation (Chowdhury et al., 2013; Wu et al., 2013; Zhao et al., 2014; Hua et al., 2015; Huang et al., 2016).

In addition, fine mineral particles are important components of sediments and soils, and inevitably they are widely present in groundwater (Han et al., 2008). In groundwater, the heteroaggregation of nanoparticles with clay minerals is a critical process for the stability of nanoparticles (Wang et al., 2015a, 2015b), and the deposition of nanoparticles onto immobile surfaces can play a dominant role. Various investigators have examined the interaction between engineered nanoparticles (e.g. Ag, TiO_2 and Al_2O_3) with clay minerals (e.g. montmorillonite, kaolinite and goethite) (Zhou et al., 2012; Labille et al., 2015; Wang et al., 2015a, 2015b; Bayat et al., 2015). These studies suggest that the surface charge and the shape of the clay particles affect the stability of engineered nanoparticles due to heteroaggregation. Consequently, the interaction between GO nanoparticles and clay minerals may be critical for the transport and retention of GO nanoparticles in porous media.

Kaolinite is one of the most common clay minerals in the subsurface, so it is possible to interact with GO nanoparticles. Zhao et al. (2015) have investigated the destabilization of GO nanoparticles via heteroaggregation with kaolinite at only one controlled condition ($T = 25$ °C, pH = 6.5) in presence of Na^+ and Ca^+, and observed that heteroaggregation was unfavorable. Huang et al. (2016) have examined the influence of pH, I_S and initial nanoparticle concentration on heteroaggregation of GO nanoparticles with kaolinite and kaolinite-goethite complex, and reported that heteroaggregation was favorable for low pH, high I_S and low GO concentrations.

The aim of this work was to investigate the effect of water chemistry and temperature on the heteroaggregation between GO nanoparticles and kaolinite colloids. Dynamic batch experiments were conducted at three controlled temperatures, using GO nanoparticles and kaolinite colloids in suspension at different pH values and ionic strengths (I_S). It is worthy to note that the selected temperature range (8–25 °C), and pH range (4–10) considered in this study, are representative of the conditions observed in various ground and surface waters (Collins, 1925). To the best of our knowledge, no previous study has investigated the effect of temperature on the heteroaggregation between GO nanoparticles and KGa-1b colloids in conjunction with the associated thermodynamics.

2. Methodology

2.1. Materials

GO suspensions were prepared by mixing the appropriate amount of GO sheets (Sigma Aldrich, St. Louis, USA) with a phosphate buffered solution (PBS) with relatively low ionic strength ($I_S = 7$ mM). Afterwards, the suspensions were sonicated (37 kHz) (Elmasonic S 30/(H), Elma Schmidbauer GmbH, Singen, Germany) for 2 h to ensure that the dispersion is thoroughly uniform, as suggested by Sotirelis and Chrysikopoulos (2015). All aggregation experiments were conducted with a concentration of GO nanoparticles of $C_{GO} = 5$ mg/L, whereas for the isotherm experiments the range of GO nanoparticles concentrations was 1–25 mg/L. However, it should be noted that concentrations of GO in environmental systems could be smaller than the 5 mg/L used in this study.

The kaolinite (KGa-1b, well-crystallized kaolin, from Washington County, Georgia) (Pruett and Webb, 1993) used in this study was purchased from the Clay Minerals Society (Columbia, Missouri, USA). KGa-1b has specific surface area (SSA) of 10.1 m^2/g, as evaluated by the Brunauer–Emmet–Teller (BET) method, and cation exchange capacity (CEC) of 2.0 meq./100 g (van Olphen and Fripiat, 1979). The <2 μm colloidal fraction, used in all of the experiments conducted in this study, was separated by sedimentation following the procedures outlined by Rong et al. (2008). Briefly, 12 g of KGa-1b were mixed with 25 mL of distilled deionized water (ddH_2O) in a 2 L beaker. Hydrogen peroxide (30% solution) was added to the suspension to oxidize organic matter, while the pH was adjusted to 10 with 0.1 M NaOH. The suspension was diluted to 2 L and the <2 μm colloid fraction was separated from larger particles by sedimentation for a time period of 1 h. The size of the colloids was confirmed using a Zeta-Sizer analyzer. Adding a 0.5 M $CaCl_2$ solution flocculated the separated colloid suspension. The colloid particles were washed with ddH_2O, ethanol and again ddH_2O, and finally dried at 60 °C. The KGa-1b suspensions were prepared by adding an appropriate amount of KGa-1b to PBS solution and sonicating for 10 min in order to obtain the desired colloidal suspension. The concentration of KGa-1b colloids used in all of the heteroaggregation experiments was $C_{KGa\text{-}1b} = 50$ mg/L.

All the solutions were prepared using ultrapure water (Easypure II, Barstead, USA) with specific resistivity of ~18.2 MΩ·cm. The various nanoparticle and colloid suspensions with different ionic strengths were adjusted with NaCl ($C_{NaCl} = 0, 5, 20$ mM for the batch experiments with $I_S = 7, 12, 27$ mM, respectively); whereas, the suspensions with different pH values were adjusted with either H_3PO_4 or NaOH. All chemicals employed in this study were of analytical reagent grade, employed without any additional purification.

The optical density of the GO nanoparticles was analyzed at the optimal wavelength of 231 nm following the procedure outlined by Liu et al. (2013). Calibration curves were prepared for each set of solution chemistry (pH and I_S) examined in this study, in order to establish the relationship between absorbance, Abs [−], and GO, in the range 0–30 mg/L. A series of diluted samples were prepared from an aqueous solution with known GO concentration, and the absorbance of each diluted sample was measured with a UV–visible spectrophotometer (Cary 400 BIO, Varian, Palo Alto, California). Furthermore, the hydrodynamic diameter and the zeta potentials of the GO nanoparticles and KGa-1b colloids under the various experimental conditions considered in this study at 25 °C were measured with a zetasizer (Nano ZS90, Malvern Instruments, Southborough, MA) (see Table 1). All zeta potential and hydrodynamic diameter measurements were obtained in triplicates.

2.2. Batch experiments

Dynamic batch experiments were conducted under various solution chemistry conditions at 8, 14, and 25 °C, in order to examine the effect of pH, I_S, and temperature on GO and KGa-1b heteroaggregation. All batch

Table 1
Measured zeta potentials and hydrodynamic diameters of GO nanoparticles and KGa-1b colloids for the different experimental conditions (Here $C_{GO} = 10$ mg/L, and $C_{KGa\text{-}1b} = 100$ mg/L).

Experimental Conditions			GO	KGa-1b	GO	KGa-1b
pH	I_S (mM)	T (°C)	Zeta potential (mV)	Zeta potential (mV)	Hydrodynamic diameter (nm)	Hydrodynamic diameter (nm)
7	7	8	−35.0	−51.0	478 ± 29	505 ± 38
7	7	14	−33.0	−50.4	492 ± 26	530 ± 41
4	7	25	−25.6	−38.8	492 ± 38	646 ± 53
7	7	25	−35.2	−50.8	465 ± 25	558 ± 40
10	7	25	−40.4	−53.9	392 ± 27	503 ± 25
7	12	25	−32.9	−49.9	503 ± 34	629 ± 33
7	27	25	−30.3	−48.6	558 ± 41	686 ± 48

experiments were performed in 20 mL Pyrex glass screw-cap tubes (Fisher Scientific). Glass tubes were washed with detergent, rinsed thoroughly in ddH_2O, autoclave sterilized, and oven-dried at 80 °C overnight. A PBS solution with $I_S = 7$ mM was prepared with 0.004 M phosphate buffer salts in ddH_2O and adjusted to a pH = 7.2 with NaOH. The PBS solution was used to stabilize the pH of GO dispersion (Dreyer et al., 2010). All the experiments were performed with the tubes attached to a rotator (Selecta, Agitador orbit), operated at 12 rpm, in order to allow for KGa-1b to mix within the GO suspension. The experiments at 8 and 14 °C were conducted in an incubator (Foc 120E, Velp Scientifica, Italy).

For each experiment, 16 glass tubes were employed, which were divided into two groups. Each group consisted of eight glass tubes. The glass tubes of the first group (experimental tubes) contained a mixture of 10 mL of GO suspension ($C_{GO} = 10$ mg/L) and 10 mL of KGa-1b suspension ($C_{KGa\text{-}1b} = 100$ mg/L), and the second group (GO control tubes) contained 20 mL of GO suspension ($C_{GO} = 5$ mg/L). All glass tubes were filled to the top. Both groups of glass tubes were treated in the same manner. All used glass tubes were discarded.

For the kinetic attachment experiments, a sample was collected (10 mL) from each glass tube at different preselected times (0, 5, 10, 30, 60, 120, 180, 240, 360 min). For the equilibrium attachment experiments eight glass tubes with different initial GO concentration were employed, all samples were collected 60 min after the initiation of the experiment, which was sufficient time to reach equilibrium. Then, following the procedure outlined by Zhao et al. (2015), the separation of GO nanoparticles and KGa-1b colloids was made after centrifugation (3500 rpm or 1900 × g, 30 min) of each sample. The GO concentration was measured in triplicates. Note that the control tubes were used to monitor GO aggregation and possible GO attachment onto the walls of the glass tubes. All concentration calculations were made under the assumption that during centrifugation, identical amounts of suspended GO nanoparticles were settled in the GO control tubes and the experimental tubes containing also KGa-1b colloids. A schematic illustration of the experimental procedures is presented in Fig. 1.

2.3. Aggregation and heteroaggregation kinetics

The kinetics of aggregation and heteroaggregation were investigated in this study with the procedures developed by Zhou et al. (2012), and Wang et al. (2015a, 2015b). Time-resolved hydrodynamic size data of the various particle suspensions were measured using dynamic light scattering (DLS) (Nano ZS90, Malvern Instruments, Southborough, MA). The I_S of the suspension was adjusted with NaCl (0.025–0.250 M). The DLS measurements were initiated immediately after the mixing of the NaCl solution with the particle suspension. The size of aggregates was estimated every 5 min for a period of 1 hour or until the initial particle size had doubled. All DLS measurements were conducted at 25 °C.

3. Theoretical considerations

3.1. Equilibrium and kinetic GO attachment

The experimental data from the equilibrium attachment of GO onto KGa-1b at three different temperatures where fitted with a Freundlich isotherm:

$$C_{eq}^{*} = K_f C_{eq}^{m} \quad (1)$$

which can also be written in the following linear form:

$$\log C_{eq}^{*} = \log K_f + m \ \log C_{eq} \quad (2)$$

where C_{eq} [mg GO/Liter of solution] is the aqueous phase GO

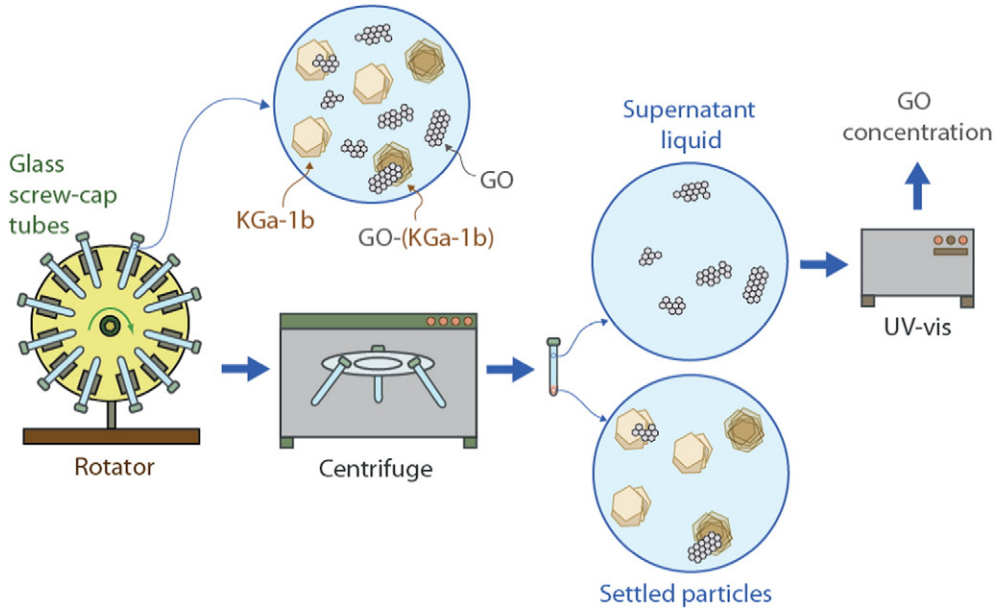

Fig. 1. Schematic illustration of the experimental procedure.

concentration at equilibrium; C_{eq}^* [mg GO/g KGa-1b] is the GO concentration attached onto the KGa-1b colloids at equilibrium; K_f [$L^{3+m}/M_s M_n^{m-1}$] is the Freundlich constant in units of [(Liter of solution)^m/(g KGa-1b)(mg GO)$^{m-1}$] and is directly proportional to the deposition and attachment capacity of the KGa-1b colloids; m [−] is the Freundlich exponent, which is equal to one for linear attachment and is a measure of the surface heterogeneity of the KGa-1b colloids (the smaller the value of m the higher the surface heterogeneity of the KGa-1b colloids). Also, for notational convenience M_n was introduced for the mass of nanoparticles (GO), and M_s, for the mass of solids (KGa-1b colloids). The parameters m and $\log K_f$ were estimated by the slope and ordinate (vertical axis intercept), respectively, of the linear plot of the experimental data in the form of $\log C_{eq}^*$ versus $\log C_{eq}$.

The experimental data from the kinetic attachment batch experiments were fitted with the following pseudo-second-order expression (Ho, 2006; Anagnostopoulos et al., 2012):

$$\frac{dC_t^*}{dt} = k_{p2}\left(C_{eq}^* - C_t^*\right)^2 \tag{3}$$

where t [t] is time; C_t^* [M_n/M_s] is the GO concentration attached onto KGa-1b at time t; and k_{p2} [$M_s/(M_n \cdot t)$] is the rate constant of the pseudo-second order attachment. Separating variables and integrating the time variable from 0 to t, and the GO concentration attached onto KGa-1b from 0 to C_t^* yields:

$$C_t^* = \frac{\left(C_{eq}^*\right)^2 k_{p2} t}{1 + C_{eq}^* k_{p2} t} \tag{4}$$

The above expression can be rearanged in a linear form:

$$C_t^* = \frac{t}{\left[1/k_{p2}\left(C_{eq}^*\right)^2\right] + \left[t/C_{eq}^*\right]} \tag{5}$$

or can also be written in the following linear form:

$$\frac{t}{C_t^*} = \frac{1}{k_{p2}\left(C_{eq}^*\right)^2} + \frac{t}{C_{eq}^*} \tag{6}$$

Pseudo-second-order kinetic models are associated with physicochemical interactions such as chemisorption (Ho, 2006), and have been used successfully to describe the kinetics of *Bacillus subtilis* attachment onto single-walled carbon nanotubes (Upadhyayula et al., 2009), the kinetics of *P. putida* attachment onto kaolinite (Vasiliadou and Chrysikopoulos, 2011), as well as the attachment of GO onto quartz sand (Sotirelis and Chrysikopoulos, 2015).

3.2. Attachment efficiency

The attachment efficiency, α [−], which is also known as the inverse stability ratio, 1/W, represents the ratio of the coagulation rate in the presence of an energy barrier to the coagulation rate in the absence of an energy barrier (Elimelech et al., 1995). Therefore, α can easily be calculated by applying the following expression to experimental coagulation kinetic data (Mylon et al., 2004; Zhou et al., 2012):

$$\alpha = \frac{1}{W} = \frac{(dr_H/dt)|_{t\to 0}}{(dr_H/dt)|_{t\to 0,\ \text{rapid}}} \tag{7}$$

where r_H [L] is the mean hydrodynamic radius of the aggregate, which is measured experimentally; $k = (dr_H/dt)|_{t\to 0}$ [L/t] is the actual (slow) coagulation rate in the presence of an energy barrier, which is actually the slope of the linear plot of r_H versus time; and $k_{rapid} = (dr_H/dt)|_{t\to 0,\ \text{rapid}}$ [L/t] is the most rapid coagulation rate in the absence of an energy barrier, which is calculated as the average of the highest, relatively constant experimental rates at high I_S values. Increasing the I_S leads to a reduction of the energy barrier between particles (less negative) and to a reaction-limited (slow) coagulation (or aggregation) regime. When the energy barrier is eliminated, the surface charge of particles is completely screened and the resulting coagulation regime is diffusion limited (fast). It should be noted that the critical coagulation concentration (CCC) is the intersection between these regimes (Chen and Elimelech, 2006, 2007; Wang et al., 2015a, 2015b). Alternatively, CCC is the I_S at which α reaches a constant value of unity (Zhou et al., 2012). However, α can exceed unity when there exists significant attraction between particles (Chen and Elimelech, 2006; Zhou et al., 2012).

3.3. Interaction energy profiles

For the calculation of the Derjaguin–Landau–Verwey–Overbeek (DLVO) interaction energy profiles (Derjaguin and Landau, 1941; Verwey and Overbeek, 1948), the following expression was used (Loveland et al., 1996):

$$\Phi_{DLVO}(h) = \Phi_{vdW}(h) + \Phi_{dl}(h) + \Phi_{Born}(h) \tag{8}$$

where Φ_{DLVO} [J] is the total interaction energy between two surfaces (here GO and KGa-1b); Φ_{vdW} [J] is the van der Waals potential energy; Φ_{dl} [J] is the double layer potential energy; Φ_{Born} [J] is the Born potential energy; and h [m] is the separation distance between the approaching surfaces. Note that Φ_{Born} can easily be neglected if h > 1 nm. It should be noted that the Born potential energy is insignificant in aqueous systems because the presence of hydrated ions is almost certain will prevent surface-surface separation distances to diminish to the limiting value of h ~ 0.3 nm (Elimelech et al., 1995; Chrysikopoulos and Syngouna, 2012). A typical DLVO interaction energy profile is characterized by primary minimum, Φ_{min1} (deep energy "well"), the primary maximum, Φ_{max1} (energy barrier to attachment and detachment), and the secondary minimum, Φ_{min2} (shallow energy "well") (Syngouna and Chrysikopoulos, 2011; Chrysikopoulos et al., 2012).

For the case of two approaching surfaces, one with spherical (GO) and the other with planar (KGa-1b) geometries, the GO−(KGa-1b) interactions were assumed to be of the sphere-plate type. Therefore, the Φ_{vdW} [J] for GO−(KGa-1b) (sphere-plate) interactions were calculated with the expression (Lyklema, 1991; Voorn et al., 2007):

$$\Phi_{vdW}(h) = -\frac{A_{123}}{6}\left[\frac{2r_p(h+r_p)}{h(h+2r_p)} + \ln\left(\frac{h}{h+2r_p}\right)\right] \tag{9}$$

where r_p [L] is particle radius; and A_{123} [J] is the combined Hamaker constant for microscopic bodies of composition "1" and "3" in medium "2" [(1-GO particle)-(2-water)-(3-KGa-1b)] and can be estimated by the geometric mean combining rule (Yoon et al., 1997):

$$A_{123} = \sqrt{A_{121}A_{323}} \tag{10}$$

In this study, the combined Hamaker constants for the system GO–water–GO was set to $A_{121} = 2.23 \times 10^{-21}$ J (McAllister et al., 2007) and for the system (KGa-1b)–water–(KGa-1b) to $A_{323} = 3.1 \times 10^{-20}$ J (Chrysikopoulos and Syngouna, 2012). Consequently, in view of Eq. (12), $A_{123} = 8.31 \times 10^{-21}$ [J]. Furthermore, the Φ_{dl} [J] GO−(KGa-1b) (sphere-plate) interactions were calculated with the expression (Voorn et al., 2007):

$$\Phi_{dl}(h) = \pi\varepsilon_r\varepsilon_0 r_p\left[\left(\Psi_1^2 + \Psi_2^2\right)\ln\left(\frac{\exp(2\kappa h)-1}{\exp(2\kappa h)}\right) + 2\Psi_1\Psi_2\ln\left(\frac{\exp(\kappa h)+1}{\exp(\kappa h)-1}\right)\right] \tag{11}$$

where Ψ_1 [V] is the Stern potential of the GO nanoparticle; Ψ_2 [V] is the Stern potential of the KGa-1b surface; and κ [1/m] is the inverse of the effective diffuse double layer thickness, known as the

Debye-Huckel length:

$$\kappa = \left[\frac{2000\ I_S N_A e^2}{\varepsilon_r \varepsilon_0 k_B T}\right]^{1/2} \tag{12}$$

where I_S [mol/L] is the ionic strength, $N_A = 6.02 \times 10^{23}$ [1/mol] is Avogadro's number, and $e = 1.602 \times 10^{-19}$ [C] is the elementary charge; $\varepsilon_r = \varepsilon/\varepsilon_0$ is the dimensionless relative dielectric constant of the suspending liquid; ε [$C^2/(J \cdot m)$] is the dielectric constant of the suspending liquid; ε_0 [$C^2/(J \cdot m)$] is the permittivity of free space; $k_B = 1.38 \times 10^{-23}$ [J/K] is the Boltzmann constant; and T [K] is the fluid absolute temperature.

For the case of two approaching surfaces, both with planar (KGa-1b) geometries, the (KGa-1b)-(KGa-1b) interactions were assumed to be of the plate-plate type. Therefore, the Φ_{vdW} [J] for (KGa-1b)-(KGa-1b) (plate-plate) interactions were calculated with the following expression (Elimelech et al., 1995):

$$\Phi_{vdW}(h) = -\frac{A_{123}}{12\pi h^2} \tag{13}$$

Furthermore, the Φ_{dl} [J] for (KGa-1b)-(KGa-1b) (plate-plate) interactions were calculated with the expression (Verwey and Overbeek, 1948):

$$\Phi_{dl}(h) = \frac{32 n_\infty k_B T}{\kappa}\gamma^2[1 - \tanh(\kappa h)] \tag{14}$$

where n_∞ is the bulk number density of ions given by (Elimelech et al., 1995, p.36):

$$n_\infty = 1000 N_A C_s \tag{15}$$

where C_s [mol/dm^3] is the salt concentration or electrolyte molar concentration (decimeter: dm = 10 cm), and γ [−] is a dimensionless function of the surface potential, defined as (Gregory, 1975; Elimelech et al., 1995, p.172):

$$\gamma = \tanh\left(\frac{ze\psi}{4k_B T}\right) \tag{16}$$

where Ψ [V] is the Stern potential, and z [−] is the ion valence including the sign of the ion charge. In this study, the zeta potential is used as an estimate of Stern potential.

For the case of two approaching surfaces, both with spherical (GO) geometries, the GO-GO interactions were assumed to be of the sphere-sphere type. Note that in the present study it is assumed that because of the sample mixing by rotation, the GO sheets may be folded and their geometry could be spherical or hemi-spherical (Huang et al., 2016). Therefore, the Φ_{vdW} [J] GO-GO (sphere-sphere) interactions were calculated with the following expression (Elimelech et al., 1995, p.44):

$$\Phi_{vdW}(h) = -\frac{A_{323} r_{p1} r_{p2}}{6h(r_{p1} + r_{p2})} \tag{17}$$

where r_{p1} [L] and r_{p2} [L] is the radius of particles 1 and 2, respectively. Note that the above equation is valid for $h \ll r_{p1}$. Furthermore, the Φ_{dl} [J] for GO-GO (sphere-sphere) (identical spheres) interactions were calculated with the expression (Elimelech et al., 1995, p.39):

$$\Phi_{dl}(h) = 32\pi\varepsilon r_p \left(\frac{k_B T}{ze}\right)^2 \gamma^2 \exp(-\kappa h) \tag{18}$$

3.4. Thermodynamic considerations

The thermodynamic behavior of GO nanoparticle attachment onto KGa-1b colloids was investigated by estimating the standard Gibbs free energy change, ΔG° [kJ/mol], the standard enthalpy change, ΔH° [kJ/mol], and the standard entropy change, ΔS° [J/mol·K] from the temperature dependent attachment isotherms, as outlined by Sotirelis and Chrysikopoulos (2015). The ΔG° at a selected temperature can be determined from the following thermodynamic relationship:

$$\Delta G^\circ = -R_a T\ \ln K_0 \tag{19}$$

where $R_a = 8.3145$ [J/(mol·K)] is the universal gas constant; and K_0 [L^3/M] is the thermodynamic attachment equilibrium constant, also known as the thermodynamic distribution coefficient, which can be determined from the intercept with the vertical axis of the linear plot of $\ln[C_{eq}^*/C_{eq}]$ versus C_{eq}^* (Biggar and Cheung, 1973; Khan and Singh, 1987). Furthermore, the values of ΔH° and ΔS° can be obtained from the following thermodynamic relationship:

$$\ln K_0 = \frac{\Delta S^\circ}{R_a} - \frac{\Delta H^\circ}{R_a T} \tag{20}$$

The slope and vertical axis intercept (ordinate) of a linear plot of $\ln K_o$ versus 1/T correspond to the $\Delta H^\circ/R_a$ and $\Delta S^\circ/R_a$, respectively.

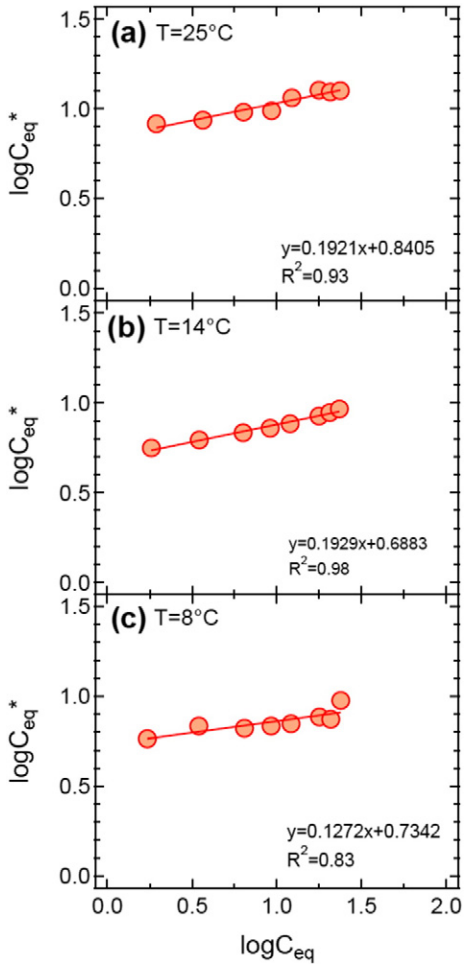

Fig. 2. Linearized Freundlich isotherms for GO nanoparticles attachment onto KGa-1b colloids at three different temperatures: (a) 25 °C, (b) 14 °C, and (c) 8 °C.

Table 2
Calculated Freundlich parameters for GO attachment onto KGa-1b.

T (°C)	m (−)	K_f [L^m/(g KGa-1b)(mg GO)$^{m-1}$]
25	0.1921	6.93
14	0.1929	4.88
8	0.1272	5.42

Table 3
Fitted parameters obtained from the GO kinetic attachment experiments.

Experimental conditions			C^*_{eq} [mg GO/g KGa-1b]	k_{p2} [g KGa-1b/(mg GO·min)]
pH	I_S (mM)	T (°C)		
4	7	25	9.56	0.085
7	7	25	7.85	0.293
10	7	25	7.13	2.217
7	12	25	8.47	53.36
7	27	25	14.70	0.038
7	7	8	6.04	0.262
7	7	14	7.66	0.096

4. Results and discussion

The equilibrium attachment data from the dynamic experiments of GO nanoparticles attachment onto KGa-1b colloids at three different temperatures are shown in Fig. 2. The equilibrium attachment data were fitted with linear, Freundlich, and Langmuir isotherm models. However, only the Freundlich isotherm model fittings, constructed by the graphical statistical software "IGOR-Pro" (WaveMetrics Inc.), are shown in Fig. 2, and the corresponding Freundlich isotherm parameters are listed in Table 2. Also, the K_f values listed in Table 2 suggested that, for most of the cases examined in this study, the attachment of GO nanoparticles increased with increasing temperature.

The data from the kinetic batch experiments under the various experimental conditions considered in this study are presented in Fig. 3. The fitted kinetic model-parameter values for k_{p2} are listed in Table 3. Furthermore, the pseudo-second-order model (Eq. (4)) was fitted to the kinetic experimental data with the nonlinear least squares regression software ColloidFit (Katzourakis and Chrysikopoulos, 2016), which incorporates the state of the art model-independent parameter estimation package "Pest" (Doherty et al., 1994). Fig. 3a shows the influence of pH on GO nanoparticles attachment onto KGa-1b colloids. The observed decrease in GO nanoparticle mass attached onto KGa-1b with increasing pH values is attributed to the structure of the KGa-1b colloids. Note that at pH 4 the Al-O face/edge of KGa-1b is positive charged (Wang et al., 2015a, 2015b), so more GO nanoparticles, which were negatively charged at pH = 4, were expected to be attracted to Al-O face/edge. However, for greater pH values, Al-O faces and Si-O faces of KGa-1b, carry negative charges (Wang et al., 2015a, 2015b). Fig. 3b shows that increasing I_S leads to a significant increase in the attachment of GO nanoparticles onto KGa-1b colloids. Note that increasing I_S leads to smaller absolute zeta potential values (see Table 1) and consequently, to smaller electric double layer repulsion (Chen and Elimelech, 2007) between GO nanoparticles and KGa-1b colloids. Fig. 3c shows the influence of temperature on the attachment of GO nanoparticles onto KGa-1b colloids. The experimental data suggest that there is a slight decrease in GO attachment with decreasing temperature. Furthermore, for all cases examined in this work, the attachment of GO nanoparticles onto KGa-1b colloids was relatively fast, reaching equilibrium within 10 to 20 min (see Fig. 3).

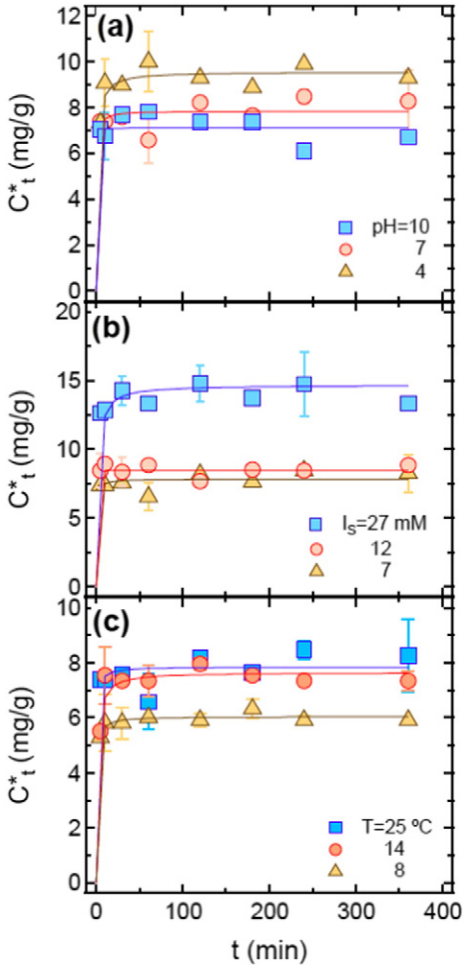

Fig. 3. Effect of (a) pH at I_S = 7 mM and T = 25 °C, (b) I_S at pH = 7 and T = 25 °C, and (c) temperature at pH = 7 and I_S = 7 mM, on kinetic attachment of GO onto KGa-1b. The symbols represent the experimental data, and the curves the fitted model simulations.

The influence of I_S on the aggregation of KGa-1b colloids, GO nanoparticles, and heteroaggregation of GO−(KGa-1b) at pH = 7 is illustrated graphically in Fig. 4, and the corresponding $k = (dr_H/dt)|_{t\to 0}$ and $k_{rapid} = (dr_H/dt)|_{t\to 0,\ rapid}$ values are listed in Table 4. Furthermore, Fig. 5 presents a few, randomly selected, linear plots with slopes equal to the k values listed in Table 4. The slope of each linear plot in Fig. 5 is determined with the graphical statistical software "IGOR-Pro" (WaveMetrics Inc.), and equals to the corresponding k with units (nm/s). The k_{rapid} values listed in Table 4 are calculated by averaging all the corresponding k values for the cases where there is no energy barrier (Φ_{max1}). Note that all three systems exhibited high stability. It should be noted that for I_S < 25 mM the attachment efficiency for

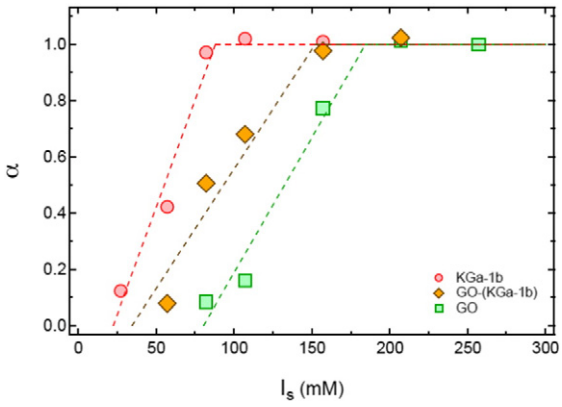

Fig. 4. Attachment efficiencies, α (or Inverse stability ratios, 1/W) of (KGa-1b)–(KGa-1b) (circles), GO–GO (squares), and GO–(KGa-1b) (diamonds) as a function of NaCl concentration at pH 7. The CCC (intersection of reaction-limited (slow) and diffusion limited (fast) coagulation regimes) for (KGa-1b)–(KGa-1b) is 88 mM NaCl, for GO–GO is 184 mM NaCl, and for GO–(KGa-1b) is 152 mM NaCl.

Table 4
Calculated k and k_{rapid} values for the various aggregation and heteroaggregation experiments (Here $C_{GO} = 5$ mg/L and $C_{KGa\text{-}1b} = 50$ mg/L).

Experimental conditions (pH = 7, $T = 25$ °C)	$k_{rapid} = (dr_H/dt)\|_{t\to 0,\ rapid}$ (nm/s)		
	GO	KGa-1b	GO−(KGa-1b)
	1.79	1.89	1.61
I_S (mM)	$K = (dr_H/dt)\|_{t\to 0}$ (nm/s)		
27	–	0.23[a]	–
57	–	0.80	0.13[a]
82	0.15[a]	1.83[b]	0.81
107	0.29	1.93[b]	1.09
157	1.39	1.91[b]	1.58[b]
207	1.81	–	1.64[b]
257	1.79[b]	–	–

[a] For k calculation refer to Fig. 5.
[b] Without energy barrier, as predicted by the classical DLVO theory.

these three systems was very small. The GO suspension was the most stable with CCC = 184 mM, caused by high electrostatic repulsion between GO nanoparticles (Gregory, 2006; Chowdhury et al., 2013). Also, stable was the KGa-1b suspension with CCC ≈ 88 mM, but less stable than GO, probably due to the larger size of the KGa-1b colloids. The GO−(KGa-1b) suspension was very stable with CCC = 152 mM. Therefore, the presence of KGa-1b colloids destabilize lightly the GO suspension; whereas, GO nanoparticles enhance the stability of KGa-1b (see Table 4). The observed high stability of GO−(KGa-1b) is attributed to the high negative charge of both GO nanoparticles (−35.2 mV) and KGa-1b colloids (−50.8 mV) as recorded for neutral pH and low I_S values. Therefore, the GO and KGa-1b heteroaggregation at low NaCl concentration is expected to be very small. Note that increasing I_S values until they reach CCC, leads to a decrease of the energy well (Φ_{max1}), so the heteroaggregation of GO nanoparticles with KGa-1b colloids is more favorable.

The measured zeta potential values of GO and KGa-1b (see Table 1) indicate that both GO and KGa-1b are negatively charged over the pH range (4 ≤ pH ≤ 10) examined in this study, and suggest that the interactions between GO and KGa-1b are repulsive. The absolute zeta potential value of both GO and KGa-1b suspensions decreased, or equivalently the zeta potential values became less negative, with increasing I_S, due to suppression of the electric double layer (Feriancikova and Xu, 2012; Lanphere et al., 2013). The experimental data clearly show that decreasing the pH contributed to a decrease in the absolute zeta potential values, as result of the reduction in the electrostatic repulsive forces, as predicted by the classical DLVO colloidal theory (Derjaguin and Landau, 1941; Verwey and Overbeek, 1948). Furthermore, the zeta potential values were consistently greater for GO than KGa-1b particles.

The Φ_{DLVO} sphere-plate interaction energy profiles for GO−(KGa-1b) under the present experimental conditions are presented in Fig. 6. Clearly, these interaction energy profiles suggest that for normal conditions (neutral pH and low I_S values) there is a shallow Φ_{min2}, and a relatively high Φ_{max1}, indicating the presence of strong repulsive forces between GO nanoparticles and KGa-1b colloids. As a result, a reduction in pH yielded smaller Φ_{max1} and small deepening in the Φ_{min2} (see Fig. 6a). Furthermore, an increase in I_S resulted a small reduction in Φ_{max1}, and a small deepening in Φ_{min2} for smaller separation distance (see

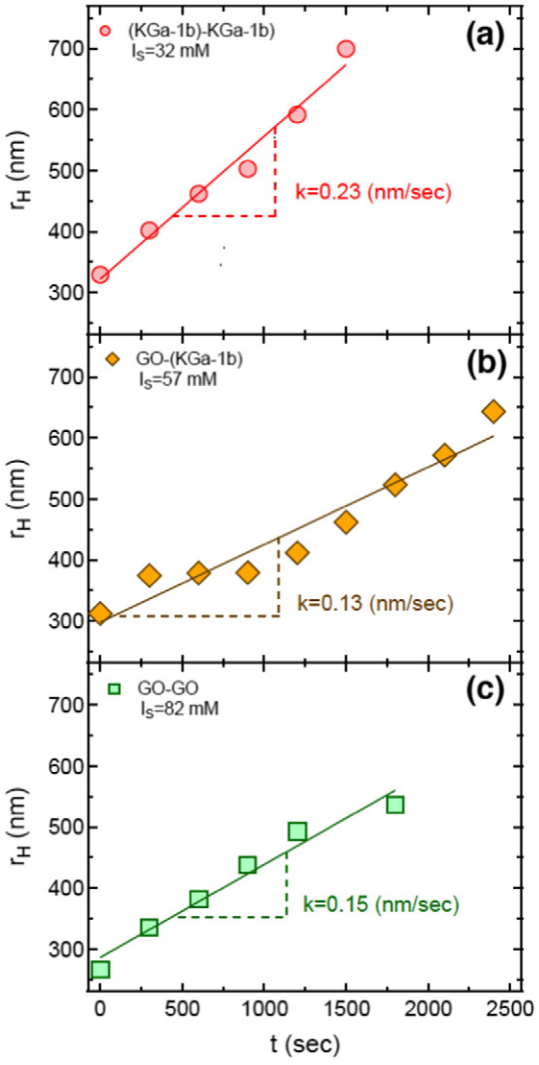

Fig. 5. Behavior of r_H as a function of time for: (a) (KGa-1b)–(KGa-1b) at $I_S = 32$ mM, (b) GO–(KGa-1b) at $I_S = 57$ mM, and (c) GO–GO at $I_S = 82$ mM (Here pH = 7 and $T = 25$ °C).

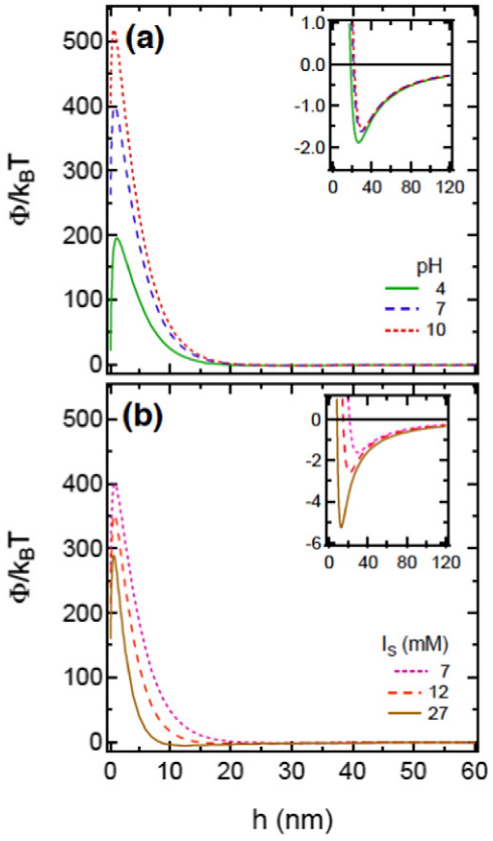

Fig. 6. Predicted DLVO total interaction energy profiles between GO and KGa-1b, as a function of separation distance for the experimental conditions. Each figure insert highlights the corresponding secondary energy minima.

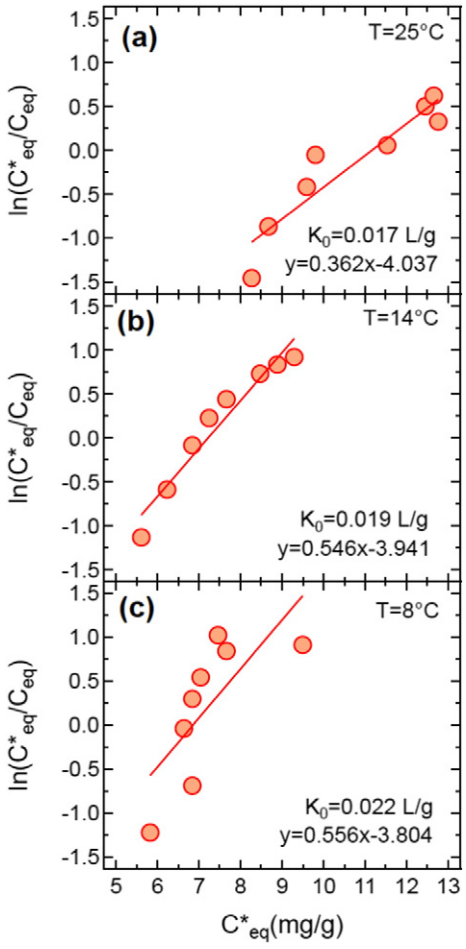

Fig. 7. Linear plots of $\ln[C^*_{eq}/C_{eq}]$ versus C^*_{eq} at three different temperatures: (a) 25 °C, (b) 14 °C, and (c) 8 °C. K_0 is the intercept of the fitted line with the vertical axis.

Fig. 6b). These findings are in agreement with the results from the batch experiments of this study. For a deeper secondary energy minimum ($I_S = 27$ mM) greater attachment was observed. Nevertheless, the attachment of the GO nanoparticles onto KGa-1b colloids cannot be fully attributed to the deepening of Φ_{min2}. It is worthy to note that, predictions of energy barriers and secondary energy minima are strongly dependent on the model selected for electrostatic double layer interaction calculations. Also, the interaction forces were intentionally calculated for h > 0.3 nm, rendering the effect of Born interaction as insignificant. Consequently, the interaction energy profiles constructed in Fig. 6 do not exhibit a Φ_{min1}. Interactions between solid surfaces in water can be described well by the DLVO model for most systems at h ≥ 10 nm. For smaller h values, non-DLVO forces often yield strong interaction forces that can prevent primary well formation when the surfaces have the same charge.

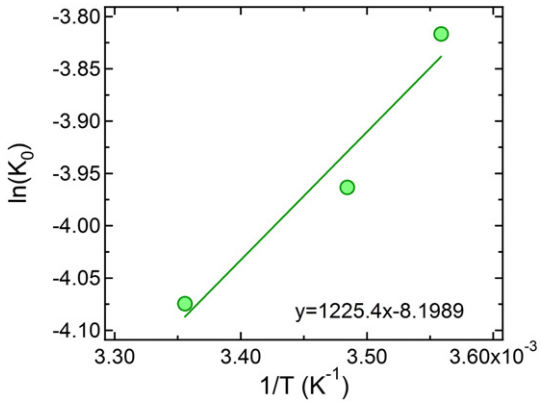

Fig. 8. Linear plot of $\ln K_0$ versus 1/T.

The values of $\Delta G° = 8.89$, 9.41, and 10.00 kJ/mol for $T = 8$, 12, and 25 °C, respectively, are estimated with Eq. (19) and K_0 from the experimental data presented in Fig. 7. Furthermore, in view of Eq. (20), $\Delta H° = -10.2$ kJ/mol and $\Delta S° = -68.2$ J/mol·K are obtained from the linear plot presented in Fig. 8. All linear regressions were obtained with the graphical statistical software "IGOR-Pro" (WaveMetrics Inc.). Note that the value of K_0 decreased with increasing temperature (see Fig. 7), suggesting that the attachment process was exothermic. The positive values of $\Delta G°$ indicated that the attachment process was non-spontaneous. The increasing $\Delta G°$ values with increasing temperature suggest that the process is not feasible at higher temperatures. Furthermore, the negative $\Delta H°$ value indicated that the attachment process was exothermic (Deepthi Rani and Sasidhar, 2012). Finally, the negative $\Delta S°$ value reflected that the attachment process was enthalpy driven with reduced randomness at the solid/liquid interface during the attachment process.

5. Conclusions

The experimental results of this study suggested that heteroaggregation between GO nanoparticles and KGa-1b colloids was not favorable. The equilibrium attachment process was adequately described by the Freundlich isotherm equation. The kinetic batch experiments have shown that the attachment of GO nanoparticles onto KGa-1b colloids followed a pseudo-second-order model. The attachment process was characterized as exothermic and non-spontaneous, indicating that the process is not favorable under normal conditions. It was demonstrated that temperature and pH did not significantly affect GO attachment onto KGa-1b. In contrast, heteroaggregation rates were considerably increased at high I_S (>50 mM) values due to a decrease of the electrical double layer repulsion.

Acknowledgements

The authors are thankful for the various suggestions and thoughtful comments provided by V.I. Syngouna. This research has been co-financed by the European Union (European Social Fund-ESF) and Greek national funds through the Operational program "Education and Lifelong Learning" of the National Strategic Reference Framework (NSRF)-Research Funding Program: Aristeia I (Code 1185).

References

Akhavan, O., Ghaderi, E., 2010. Toxicity of graphene and graphene oxide nanowalls against bacteria. ACS Nano 4 (10), 5731–5736.
Anagnostopoulos, V.A., Manariotis, I.D., Karapanagioti, H.K., Chrysikopoulos, C.V., 2012. Removal of mercury from aqueous solutions by malt spent rootlets. Chem. Eng. J. 213, 135–141.
Bayat, A.E., Junin, R., Mohsin, R., Hokmabadi, M., Shamshirband, S., 2015. Influence of clay particles on Al_2O_3 and TiO_2 nanoparticles transport and retention through limestone porous media: measurements and mechanisms. J. Nanopart. Res. 17 (219):1–14. http://dx.doi.org/10.1007/s11051-015-3031-4.
Biggar, J.W., Cheung, M.W., 1973. Adsorption of picloram (4-amino-3,5,6-trichloropicolinic acid) on panoche, ephrata, and palouse soils: a thermodynamic approach to the adsorption mechanism. Soil Sci. Soc. America J. 37 (6), 860–863.
Brar, S.K., Verma, M., Tyagi, R.D., Surampalli, R.Y., 2010. Engineered nanoparticles in wastewater and wastewater sludge—evidence and impacts. Waste Manag. 30 (3), 504–520.
Chang, Y., Yang, S.T., Liu, J.H., Dong, E., Wang, Y., Cao, A., Liu, Y., Wang, H., 2011. In vitro toxicity evaluation of graphene oxide on A549 cells. Toxicol. Lett. 200 (3):201–210. http://dx.doi.org/10.1016/j.toxlet.2010.11.016.
Chen, K.L., Elimelech, M., 2006. Aggregation and deposition kinetics of fullerene (C60) nanoparticles. Langmuir 22:10994–11001. http://dx.doi.org/10.1021/la062072v.
Chen, K.L., Elimelech, M., 2007. Influence of humic acid on the aggregation kinetics of fullerene (C60) nanoparticles in monovalent and divalent electrolyte solutions. J. Colloid Interface Sci. 309 (1), 126e134. http://dx.doi.org/10.1016/j.jcis.2007.01.074.
Chen, D., Feng, H., Li, J., 2012. Graphene oxide: preparation, functionalization, and electrochemical applications. Chem. Rev. 112 (11), 6027–6053.

Chowdhury, I., Duch, M.C., Mansukhani, N.D., Hersam, M.C., Bouchard, D., 2013. Colloidal properties and stability of graphene oxide nanomaterials in the aquatic environment. Environ. Sci. Technol. 47:6288–6296. http://dx.doi.org/10.1021/es400483k.

Chrysikopoulos, C.V., Syngouna, V.I., 2012. Attachment of bacteriophages MS2 and ΦX174 onto kaolinite and montmorillonite: extended-DLVO interactions. Colloids Surf. B: Biointerfaces 92:74–83. http://dx.doi.org/10.1016/j.colsurfb.2011.11.028.

Chrysikopoulos, C.V., Syngouna, V.I., Vasiliadou, I.A., Katzourakis, V.E., 2012. Transport of *Pseudomonas putida* in a three-dimensional bench scale experimental aquifer. Transp. Porous Media 94:617–642. http://dx.doi.org/10.1007/s11242-012-0015-z.

Chung, C., Kim, Y.-K., Shin, D., Ryoo, S.-R., Hong, B.H., Min, D.-H., 2013. Biomedical applications of graphene and graphene oxide. Acc. Chem. Res. 46 (10):2211–2224. http://dx.doi.org/10.1021/ar300159f.

Collins, W.D., 1925. Temperature of Water Available for Industrial Use in the United States. Department of the Interior, Geological Survey, Water Supply Paper 520-F, U.S.

Deepthi Rani, R., Sasidhar, P., 2012. Sorption of cesium on clay colloids: kinetic and thermodynamic studies. Aquat. Geochem. 18:281–296. http://dx.doi.org/10.1007/s10498-012-9163-6.

Derjaguin, B.V., Landau, L., 1941. Acta Physicochim. USSR 14, 633–662.

Doherty, J., Brebber, L., Whyte, P., 1994. PEST: Model-Independent Parameter Estimation. Watermark Computing, Brisbane, Australia.

Dreyer, D.R., Park, S., Bielawski, C.W., Ruoff, R.S., 2010. The chemistry of graphene oxide. Chem. Soc. Rev. 39:228–240. http://dx.doi.org/10.1039/b917103g.

Elimelech, M., Gregory, J., Jia, X., Williams, R.A., 1995. Particle Deposition & Aggregation: Measurement, Modelling and Simulation. Butterworth–Heinemann Ltd, Oxford, U.K.

Feriancikova, L., Xu, S., 2012. Deposition and remobilization of graphene oxide within saturated sand packs. J. Hazard. Mater. 235−236, 194–200.

Gottschalk, F., Sonderer, T., Scholz, R.W., Nowack, B., 2009. Modeled environmental concentrations of engineered nanomaterials (TiO_2, ZnO, Ag, CNT, fullerenes) for different regions. Environ. Sci. Technol. 43 (24), 9216–9222.

Gottschalk, F., Sonderer, T., Scholz, R.W., Nowack, B., 2010. Possibilities and limitations of modeling environmental exposure to engineered nanomaterials by probabilistic material flow analysis. Environ. Toxicol. Chem. 29 (5), 1036–1048.

Gregory, J., 1975. Interaction of unequal double layers at constant charge. J. Colloid Interface Sci. 51 (1):44–51. http://dx.doi.org/10.1016/0021-9797(75)90081-8.

Gregory, J., 2006. Particles in Water: Properties and Processes. CRC Press, Boca Raton, FL, U.S.A.

Han, Z., Zhang, F., Lin, D., Xing, B., 2008. Minerals affect the stability of surfactant-facilitated carbon nanotube suspensions. Environ. Sci. Technol. 42, 6869–6875.

Ho, Y.-S., 2006. Review of second-order models for adsorption systems. J. Hazard. Mater. 136 (3), 681–689.

Hu, C., Wang, Q., Zhao, H., Wang, L., Guo, S., Li, X., 2015. Ecotoxicological effects of graphene oxide on protozoan *Euglena gracilis*. Chemosphere 128:184–190. http://dx.doi.org/10.1016/j.chemosphere.2015.01.040.

Hua, Z., Tang, Z., Bai, X., Zhang, J., Yu, L., Cheng, H., 2015. Aggregation and resuspension of graphene oxide in simulated natural surface aquatic environments. Environ. Pollut. 205:161–169. http://dx.doi.org/10.1016/j.envpol.2015.05.039.

Huang, G., Guo, H., Zhao, J., Liu, Y., Xing, B., 2016. Effect of co-existing kaolinite and goethite on the aggregation of graphene oxide in the aquatic environment. Water Res. 102:313–320. http://dx.doi.org/10.1016/j.watres.2016.06.050.

Katzourakis, V.E., Chrysikopoulos, C.V., 2016. ColloidFit - a multipurpose fitting software for colloid fate and transport phenomena in porous media. User Manual v.1.1.1 http://dx.doi.org/10.13140/RG.2.1.1234.8405.

Keller, A., McFerran, S., Lazareva, A., Suh, S., 2013. Global life cycle releases of engineered nanomaterials. J. Nanopart. Res. 15 (6):1–17. http://dx.doi.org/10.1007/s11051-013-1692-4.

Keller, A.A., Lazareva, A., 2014. Predicted releases of engineered nanomaterials: fromglobal to regional to local. Environ. Sci. Technol. Lett. 1, 65–70.

Khan, A.A., Singh, R.P., 1987. Adsorption thermodynamics of carbofuran on Sn(IV) arsenosilicate in H^+, Na^+ and Ca^{2+} forms. Colloids Surf. 24 (1):33–42. http://dx.doi.org/10.1016/0166-6622(87)80259-7.

Kim, J., Cote, L.J., Huang, J., 2012. Two dimensional soft material: new faces of graphene oxide. Acc. Chem. Res. 45 (8):1356–1364. http://dx.doi.org/10.1021/ar300047s.

Klaine, S.J., Koelmans, A.A., Horne, N., Carley, S., Handy, R.D., Kapustka, L., Nowack, B., von der Kammer, F., 2012. Paradigms to assess the environmental impact of manufactured nanomaterials. Environ. Toxicol. Chem. 31 (1), 3–14.

Labille, J., Harns, C., Bottero, J.-Y., Brant, J.A., 2015. Heteroaggregation of titanium dioxide nanoparticles with natural clay colloids. Environ. Sci. Technol. 49 (11):6608–6616. http://dx.doi.org/10.1021/acs.est.5b00357.

Lanphere, J.D., Luth, C.J., Walker, S.L., 2013. Effects of solution chemistry on the transport of graphene oxide in saturated porous media. Environ. Sci. Technol. 47, 4255–4261.

Lanphere, J.D., Rogers, B., Luth, C., Bolster, C.H., Walker, S.L., 2014. Stability and transport of graphene oxide nanoparticles in groundwater and surface water. Environ. Eng. Sci. 31 (7):350–359. http://dx.doi.org/10.1089/ees.2013.0392.

Lightcap, I., Kamat, P.V., 2013. Graphitic design: prospects of graphene-based nanocomposites for solar energy conversion, storage, and sensing. Acc. Chem. Res. 46 (10): 2235–2243. http://dx.doi.org/10.1021/ar300248.

Liu, L., Gao, B., Wu, L., Morales, V.L., Yang, L., Zhou, Z., Wang, H., 2013. Deposition and transport of graphene oxide in saturated and unsaturated porous media. Chem. Eng. J. 229, 444–449.

Loveland, J.P., Ryan, J.N., Amy, G.L., Harvey, R.W., 1996. The reversibility of virus attachment to mineral surfaces. Colloids Surf. A. 107, 205–221.

Lyklema, J., 1991. Fundamentals of Interface and Colloid Science. Academic Press, London.

McAllister, M.J., Li, J.-L., Adamson, D.H., Schniepp, H.C., Abdala, A.A., Liu, J., Herrera-Alonso, M., Milius, D.L., Car, R., Prud'homme, R.K., Aksay, I.A., 2007. Single sheet functionalized graphene by oxidation and thermal expansion of graphite. Chem. Mater. 19, 4396–4404.

Mylon, S.E., Chen, K.L., Elimelech, M., 2004. Influence of natural organic matter and ionic composition on the kinetics and structure of hematite colloid aggregation: implications to iron depletion in estuaries. Langmuir 20:9000–9006. http://dx.doi.org/10.1021/la049153g.

Mueller, N.C., Nowack, B., 2008. Exposure modeling of engineered nanoparticles in the environment. Environ. Sci. Technol. 42 (12), 4447–4453.

Pruett, R.J., Webb, H.L., 1993. Sampling and analysis of KGa-1b well-crystallized kaolin source clay. Clay Clay Miner. 41 (4), 514–519.

Pyun, J., 2011. Graphene oxide as catalyst: application of carbon materials beyond nanotechnology. Angew. Chem. Int. Ed. 50:46–48. http://dx.doi.org/10.1002/anie.201003897.

Rong, X., Huanga, Q., He, X., Chen, H., Cai, P., Liang, W., 2008. Interaction of pseudomonas putida with kaolinite and montmorillonite: a combination study byequilibrium adsorption, ITC, SEM and FTIR. Colloids Surf. B: Biointerfaces 64, 49–55.

Sasidharana, S., Torkzabana, S., Bradford, S.A., Dillona, P.J., Cook, P.G., 2014. Coupled effects of hydrodynamic and solution chemistry on long-termnanoparticle transport and deposition in saturated porous media. Colloids and Surfaces A. 457, 169–179.

Singh, S.K., Nayak, M.K., Kumari, S., Gracio, J.J.A., Dash, D., 2011. Characterization of graphene oxide by flow cytometry and assessment of its cellular toxicity. J. Biomed. Nanotechnol. 7 (1), 30–31.

Seabra, A.B., Paula, A.J., de Lima, R., Alves, O.L., Durán, N., 2014. Nanotoxicity of graphene and graphene oxide. Chem. Res. Toxicol. 27 (2):159–168. http://dx.doi.org/10.1021/tx400385x.

Sotirelis, N.P., Chrysikopoulos, C.V., 2015. Interaction between graphene oxide nanoparticles and quartz sand. Environ. Sci. Technol. 94 (22):13413–13421. http://dx.doi.org/10.1021/acs.est.5b03496.

Syngouna, V.I., Chrysikopoulos, C.V., 2011. Transport of biocolloids in water saturated columns packed with sand: effect of grain size and pore water velocity. J. Contam. Hydrol. 126, 301–314.

Upadhyayula, V.K.K., Deng, S., Smith, G.B., Mitchell, M.C., 2009. Adsorption of *Bacillus subtilis* on single-walled carbon nanotube aggregates, activated carbon and NanoCeram. Water Res. 43, 148–156.

Vallabani, N.V.S., Mittal, S., Shukla, R.K., Pandey, A.K., Dhakate, S.R., Pasricha, R., Dhawan, A., 2011. Toxicity of graphene in normal human lung cells (BEAS-2B). J. Biomed. Nanotechnol. 7 (1):106–107. http://dx.doi.org/10.1166/jbn.2011.1224.

van Olphen, H., Fripiat, J.J., 1979. Data Handbook for Clay Minerals and Other Non-metallic Minerals. Pergamon Press, Oxford, England, p. 346.

Vasiliadou, I.A., Chrysikopoulos, C.V., 2011. Cotransport of *Pseudomonas putida* and kaolinite particles through water saturated columns packed with glass beads. Water Resour. Res. 47 (2), W02543. http://dx.doi.org/10.1029/2010WR009560.

Verwey, E.J.W., Overbeek, J.T.G., 1948. Theory of the Stability of Lyophobic Colloids. Elsevier, Amsterdam, The Netherlands, p. 205.

Voorn, D.J., Ming, W., Laven, J., Meuldijk, J., de With, G., van Herk, A.M., 2007. Plate–sphere hybrid dispersions: heterocoagulation kinetics and DLVO evaluation. Colloids Surf. A Physicochem. Eng. Asp. 294 (1–3):236–246. http://dx.doi.org/10.1016/j.colsurfa.2006.08.022.

Wang, K., Ruan, J., Song, H., Zhang, J., Wo, Y., Guo, S., Cui, D., 2011. Biocompatibility of graphene oxide. Nanoscale Res. Lett. 6 (1):1–8. http://dx.doi.org/10.1007/s11671-010-9751-6.

Wang, H., Adeleye, A.S., Huang, Y., Li, F., Keller, A.A., 2015a. Heteroaggregation of nanoparticles with biocolloids and geocolloids. Adv. Colloid Interf. Sci. 226:24–36. http://dx.doi.org/10.1016/j.cis.2015.07.002.

Wang, H., Dong, Y.N., Zhu, M., Li, X., Keller, A.A., Wang, T., Li, F., 2015b. Heteroaggregation of engineered nanoparticles and kaolin clays in aqueous environments. Water Res. 80:130–138. http://dx.doi.org/10.1016/j.watres.2015.05.023.

Wu, L., Liu, L., Gao, B., Muñoz-Carpena, R., Zhang, M., Chen, H., Zhou, Z., Wang, H., 2013. Aggregation kinetics of graphene oxides in aqueous solutions: experiments, mechanisms, and modeling. Langmuir 29, 15174–15181.

Yoon, R.-H., Flin, D.H., Rabinovich, Y.I., 1997. Hydrophobic interactions between dissimilar surfaces. J. Colloid Interface Sci. 185, 363–370.

Zhao, J., Wang, Z., White, J.C., Xing, B., 2014. Graphene in the aquatic environment: adsorption, dispersion, toxicity and transformation. Environ. Sci. Technol. 48 (17): 9995–10009. http://dx.doi.org/10.1021/es5022679.

Zhao, J., Liu, F., Wang, Z., Cao, X., Xing, B., 2015. Heteroaggregation of graphene oxide with minerals in aqueous phase. Environ. Sci. Technol. 49 (5):2849–2857. http://dx.doi.org/10.1021/es505605w.

Zhou, D.X., Abdel-Fattah, A.I., Keller, A.A., 2012. Clay particles destabilize engineered nanoparticles in aqueous environments. Environ. Sci. Technol. 46 (14):7520–7526. http://dx.doi.org/10.1021/es3004427.

Zhou, D.D., Jiang, X.H., Lu, Y., Fan, W., Huo, M.X., Crittenden, J.C., 2016. Cotransport of graphene oxide and Cu(II) through saturated porous media. Sci. Total Environ. 550, 717–726.